ELSEVIER

Catalysis Today 33 (1997) 263–278

CATALYSIS TODAY

Zeolite encapsulated vanadium oxo species for the catalytic reduction of NO by NH_3

Robert C. Adams [a], Langqiu Xu [b], Karin Moller [b], Thomas Bein [b,*], W. Nicholas Delgass [a,*]

[a] *Purdue University School of Chemical Engineering, West Lafayette, IN 47907, USA*
[b] *Department of Chemistry, Purdue University School of Chemical Engineering, West Lafayette, IN 47907, USA*

Abstract

Vanadium oxo species have been introduced into the supercages of Y-zeolite by adsorption and decomposition of $VOCl_3$ to produce catalysts for the study of the effects of oxo vanadium site isolation on catalytic reduction of NO with NH_3. ^{51}V solid-state MAS-NMR of calcined samples with up to 4 V atoms per supercage show that Y-zeolite stabilizes vanadium with octahedral, V_2O_5-like square pyramidal, and most commonly, tetrahedral coordinations. Two distinct isolated tetrahedral environments were identified with NMR resonances around −530 and −830 ppm. There was no NMR evidence for oxygen bridge-bonded vanadia structures in the tetrahedral species in these catalysts. DRIFTS shows that ammonia adsorbs primarily on Brønsted acid sites associated with both the zeolite and the vanadium oxo species. DRIFTS during NO reaction with preadsorbed NH_3 shows the production of a hydroxyl species at 3690 cm^{-1}, which was assigned to V^{+4}–OH, in agreement with the literature. Turnover frequencies, based on NO conversion and total vanadium loading, range from 1×10^{-5} to 3×10^{-4} s^{-1} with selectivity to N_2 of 90–100%. Steady-state reaction experiments indicate that isolated vanadia species are viable sites for the catalytic reduction of NO.

1. Introduction

Nitrogen oxides, a class of gases commonly found in the emissions of combustion processes, are considered to be environmental pollutants. One of the most popular techniques for the post-combustion catalytic removal of NO_x from commercial stationary sources is selective catalytic reduction (SCR) with NH_3 over a supported vanadia catalyst [1]. In this reaction, the nitrogen oxides are reduced by NH_3 producing N_2 and H_2O. Vanadium pentoxide is chosen from the many catalysts available for this reaction due to its high activity at low temperatures, 100–400°C, high selectivity to N_2, and its resistance to poisoning by SO_x commonly found in combustion emissions [1]. Despite general agreement on many aspects of the SCR mechanism, there are several issues which have not been settled experimentally. Activity is not the only concern. There are also questions regarding selectivity to nitrogen over N_2O, an unwanted byproduct, and there is still debate over the nature of the active vanadium species on the catalyst. It is known that there are several vana-

* Corresponding authors. Tel.: +1-317-4944059; fax: +1-317-4940805; e-mail: delgass@ecn.purdue.edu; +1-317-4945495, e-mail tbein@chem.purdure.edu

PII S0920-5861(96)00154-X

dium surface species present on the catalyst surface at reaction conditions. These include vanadyl species, both monomeric and polymeric with bridging oxygens, vanadium hydroxyl species, vanadium sites with oxygen vacancies, and several possible adspecies of NH_3 and/or NO [1–20]. The oxidation state of the vanadium center of these species has also been observed to cycle between +5 and +3. Much of the debate is over the form of the most active surface vanadium group; monomeric, dimeric, or polymeric; and whether neighboring vanadyls or hydroxyls or combinations of each are required. Went et al. [8,9] found that the aggregation of the vanadium centers into oxygen bridged chains associated with increasing vanadium loading on the catalyst support had a profound effect on the reaction properties of the catalyst. Specifically, they found that at 300°C the polyvanadate chains were about ten times more active but less selective to N_2 than the monomeric vanadyl species.

There is also debate over the nature of the activated form of adsorbed NH_3. The question as to whether the adsorbed NH_3 which is active for the reduction of NO is adsorbed on the surface as dissociatively or molecularly adsorbed NH_3, or as an NH_4^+ ion has not been fully verified experimentally. Many groups report that the active adsorbed ammonia intermediate is NH_3 chemisorbed on Lewis acid sites of either the vanadia or the support [2–11]. Many of these groups propose that the Lewis bound ammonia is activated by dissociation to form an amide or amide radical species. Other groups report that the SCR reaction requires ammonia adsorbed on Brønsted acid sites as an ammonium ion [12–21].

We have chosen vanadium-loaded zeolites as model catalysts for the SCR system. It is possible to anchor vanadium oxo species at the acid sites within the supercages of Y-zeolite by a direct condensation reaction. Isolation of the oxo structures within the supercages provides an opportunity to control the nuclearity of the vanadium species more effectively than can be done by simply varying the loading of vanadium on a support. In this way, we can investigate the dependence of the SCR catalytic properties on vanadium connectivity. The zeolite-encapsulated vanadium oxo species are characterized in this work with NMR and EXAFS, and their catalytic properties and surface chemistry are studied with DRIFTS and steady state kinetic experiments. This paper summarizes the catalytic properties including activity, selectivity, and apparent activation energy measured for NO reduction by NH_3 in the absence of gas phase oxygen for the various vanadium-loaded Y-zeolite catalysts. DRIFTS is used to monitor adsorbed ammonia and its reaction with NO while NMR and EXAFS provide symmetry and coordination information on the anchored vanadium oxo species.

2. Experimental

2.1. Vanadium-loaded zeolites

The vanadium-loaded zeolites were prepared by a solution grafting method. The host zeolite was impregnated with vanadyl chloride (Aldrich, 99%), $VOCl_3$, dissolved in CCl_4 (Mallinckrodt). A condensation reaction between a ligand of the liquid vanadium precursor and an acidic zeolite hydroxyl site is then expected to create a Si–O–V bond between the vanadium oxo species and the zeolite framework. The vanadium precursor was loaded into Y-zeolites with two different levels of initial acidity, H_2Y and H_6Y. The subscripts on the acid zeolite labels indicate the number of acid sites per supercage/sodalite cage. H_2Y was made from NaY, obtained commercially as Linde LZ-Y52 with a Si/Al ratio of 2.37, by partial cation exchange with an NH_4Cl solution containing 2 mol of NH_4^+ per mol supercage. H_6Y was obtained commercially as the NH_4^+ form of Linde LZ-Y62 with a Si/Al ratio of 2.49. The

acid form of these zeolites was prepared from the NH_4^+ form according to the following scheme:

$$\text{Room Temp} \xrightarrow[O_2\ \text{flow}]{1^\circ\text{C/min}} 100^\circ\text{C} \xrightarrow[O_2\ \text{flow}]{4\ \text{h}} 100^\circ\text{C}$$

$$\xrightarrow[O_2\ \text{flow}]{1^\circ\text{C/min}} 400^\circ\text{C} \xrightarrow[O_2\ \text{flow}]{10\ \text{h}} 400^\circ\text{C} \xrightarrow[\text{vacuum}]{5\ \text{h}} 400^\circ\text{C} \quad (1)$$

to remove NH_3, leaving protons at Brønsted acid sites as the framework counter cations.

2.1.1. Preparation of VH_xY–Cl

Prior to vanadium addition, the zeolite support was pretreated and dried according to the procedure mentioned above to obtain the desired acidity. Known amounts of the zeolite were transferred under nitrogen to a purged and dried glass reaction flask that was immersed in a water bath at 50°C. A solution containing a known amount of $VOCl_3$ in 50 ml CCl_4 (predried with CaH_2) was added into the flask under nitrogen flow. The mixture was maintained at 50°C and stirred for 20 h. After the reaction, the sample was washed with fresh solvent several times and the solvent was removed under vacuum. The dried sample was transferred back to the quartz treatment tube and heated to degas the surface. Samples were then heated in an oxygen atmosphere at temperatures up to 350°C according to the following calcination scheme:

$$\text{Room Temp} \xrightarrow[O_2\ \text{flow}]{1^\circ\text{C/min}} 120^\circ\text{C}$$

$$\xrightarrow[+4\ \text{h vac}]{8\ \text{h}\ O_2\ \text{flow}} 120^\circ\text{C} \xrightarrow[O_2\ \text{flow}]{1^\circ\text{C/min}} 350^\circ\text{C} \xrightarrow[+4\ \text{h vac}]{12\text{h}\ O_2\ \text{flow}} 350^\circ\text{C} \quad (2)$$

The materials were characterized with respect to bulk vanadium content, surface vanadium content, and framework integrity by X-ray fluorescence (XRF), X-ray photoelectron spectroscopy (XPS), and X-ray diffraction (XRD), respectively. XRF experiments were carried out on a Kevex Unispec System 7000 spectrometer employing a rhodium tube X-ray source, 0.0–10.24 keV scan range. XRD experiments were carried out on a Siemens D500 Diffractometer employing a copper tube X-ray source (λ = 1.5406 Å), and 5–55° 2Θ scan angle range. XPS spectra were collected on a Perkin–Elmer 5300 spectrometer. That system uses a position sensitive detector to improve the sensitivity of the analyzer and a Mg anode X-ray source (Mg $K\alpha_{1,2}$ = 1253.7 eV) operated at 15 kV and 300 W. Typical data collection times were around 4 h at a base pressure of about $5–8 \times 10^{-9}$ Torr. The angle between the X-ray source and the electron spectrometer is fixed at 53°. Surface vanadium concentrations were determined from V/Si and V/Al intensity ratios which were corrected for differences in cross-section with the values reported by Scofield [22].

2.2. NMR

A GE 400 MHz NMR spectrometer was used to collect the ^{51}V-NMR spectra. The NMR resonance frequency of ^{51}V within the 9.4 T magnet is 105.19 MHz. All spectra were collected in a Doty 5 mm MAS probe. Samples were placed in a zirconia rotor and kept from exposure to the moisture in the atmosphere with vespel O-ring end caps. Untreated samples were stored and loaded into the NMR rotor in a glovebox under nitrogen atmosphere. The nuclear spin quantum number for ^{51}V is 7/2 which makes ^{51}V a quadrupolar nucleus. Under normal experimental conditions, the Fourier spectrum of a radio-frequency pulse has insufficient intensity to excite outer quadrupolar satellites that are too far off resonance (> 300 kHz). This excitation selectivity can lead to intensity distortions across the powder pattern [23,24]. The distortions become more severe at larger pulse lengths. Therefore, single pulse Bloch decay experiments are typically preferred to study ^{51}V systems, since these experiments avoid the longer pulse lengths needed to generate 90° and 180° pulses for quadrupolar solid echo sequences. Although the use of Bloch decays bears the

potential of producing somewhat distorted lineshapes, pulse-length dependent studies [23,24] show that short pulse lengths of 0.5–2.0 μs yield lineshapes and intensity ratios which are essentially independent of pulse length. Typical experimental parameters used to collect ^{51}V spectra shown in this paper are: a preacquisition delay of 10 μs, pulse length of 1 μs, dwell time of 0.5 μs, relaxation delay of 0.5 s, and 2 K data points.

The preacquisition delay is used to allow the electronics of the pulse transmitter to 'ring down' before the receiver starts to collect data. This delay can be very important in systems that relax very fast because a substantial amount of the initial rotational echo may decay in 10 μs. Therefore, to avoid baseline distortions and phasing problems in spectra collected under MAS conditions, the FID has been left-shifted to the maximum of the first complete rotational echo before Fourier transformation. In order to reduce the noise folded into the spectrum, a 1 MHz bandpass filter was utilized. Spectra were collected with MAS spin rates of 5–7 kHz, or were collected with the NMR rotor static to obtain the wideline powder pattern. To compensate for the signal-to-noise associated with the low, 1–10 wt%, vanadium loading, spectra are typically signal averaged over 100 000 scans. All chemical shifts are referenced to neat liquid $VOCl_3$ (Aldrich, 99%), collected as an external standard.

2.3. Extended X-ray absorption fine structure (EXAFS)

EXAFS measurements were performed at NSLS, Brookhaven National Laboratory at beamline X-11A with a stored electron energy of 2.5 GeV and ring currents between 110–240 mA. The powdered samples (about 10 mg) were gently and homogeneously mixed in the glovebox with a small amount of degassed boron nitride and degassed, molten 1:1 n-eicosane/n-octadecane wax mixture, and sealed into a thin steel plate holder. The sample thickness was adjusted such that the total absorption did not exceed a value of $\mu x = 2$ to ensure an optimum signal-to-noise ratio. The sealed samples were kept under nitrogen until EXAFS data were collected. Vanadium K-edge data at 5.465 keV were collected at about 100 K in transmission. Vanadium foil (V–V), V_2O_5 (V–O–V), Na_3VO_4 (V–O), and the vanadium precursor were used as references to extract phase shifts and backscattering amplitudes during the standard EXAFS data analysis procedures [25].

2.4. DRIFTS

The adsorption of the reactants, NH_3 and NO, over the vanadium-loaded zeolites and unloaded acid zeolites was studied using diffuse reflectance infrared Fourier transform spectroscopy (DRIFTS). The DRIFTS spectra were collected on a Nicolet 800 FTIR spectrometer with diffuse reflectance optics and environmental sample chamber (catalytic chamber model# 0030-103) from Spectra Tech. The spectrometer was equipped with an MCT (mercury–cadmium–telluride) detector, and the spectra were signal averaged over 512 scans, at a rate of about 2.67 scans per s, with 4 cm^{-1} resolution. Zinc selenide windows (Spectra Tech) allow transmission of IR radiation into and out of the sample chamber and are resistant to water adsorption. The sample chamber, or cell, assembly is capable of exposing the sample to gas flow at a regulated sample temperature. The sample is supported in a porous cup which allows a significant fraction of the gas to flow through the loose powder as it exits the cell. A gas manifold delivers mixtures of up to four gases at various concentrations and flow rates for in situ treatment. Reactant gases were obtained from BOC Gases: NO (5000 ppm, balance He), NH_3 (5360 ppm, balance He, small H_2O impurity). Dilution of the sample in diamond powder (Spectra Tech), a nonabsorbing, reflective powder, is necessary to guarantee sufficient scattering. Dilution ratios of 5:1 (di-

amond powder:sample) by weight were used in these experiments.

Experiments on the adsorption of NH_3 and NO over loaded and unloaded zeolite materials were run by first drying the sample, diluted in diamond powder, at 400°C in flowing N_2 for 4–5 h. The sample was then cooled to 100°C in flowing N_2 and a background spectrum at each relevant temperature was collected. If a single background was used for all spectra at different temperatures, changes in the zeolite absorption/reflection properties with temperature resulted in significant baseline and intensity distortions. The sample was then exposed to the reactant gas flow at atmospheric pressure for 10–30 min until changes in sequential spectra were negligible. The sample was then flushed with flowing N_2 for the remainder of the experiment. The temperature of the sample was then increased in intervals of 50°C with spectra collected at each step for about 15–30 min until changes in sequential spectra were negligible.

2.5. Steady-state reactions

Steady state activity and selectivity of the calcined vanadium-loaded zeolite catalysts were determined at temperatures of 350, 400, and 450°C. Reactions were run in a 6 mm ID, quartz U-tube reactor with catalyst loadings between 70–200 mg. A plug of glass wool was inserted into the U-tube reactor as a means of supporting the catalyst in the tube, and another plug was then placed within the tube on top of the catalyst for stability as well as a means of preheating the incoming reactant gases. Isothermal conditions were maintained with a fluidized sand bath. Typical reactant concentrations were 2500 ppm NO, 2600 ppm NH_3, balance He, with total gas flow rates of 70–75 sccm. Reactant flow rates were controlled with Matheson mass flow controllers. All steady state kinetic experiments presented in this paper were conducted in the absence of gas phase oxygen. Reactant and product stream concentrations were determined by gas chromatography with a packed column (Haysep Q: $10' \times 1/8''$, Suppelco) and the following temperature profile:

$$34°C \xrightarrow[1.5\ \text{min}]{\text{hold}} 34°C \xrightarrow[1.67\ \text{min}]{40°C/\text{min}} 100°C \xrightarrow[3.33\ \text{min}]{\text{hold}} 100°C \tag{3}$$

Activities of the catalysts with different vanadium loadings were compared by calculating the turn-over-frequency (TOF, s^{-1}) of each catalyst, defined as the moles of NO converted per mol of vanadium per s. Rate calculations were based on the assumption that the reactor could be modeled as an integral plug flow reactor and that the rate of reaction may be expressed as

$$-r_{NO} = k' C^1_{NO} C^0_{NH_3} = k C_{NO} \tag{4}$$

where r_{NO} and k are the rate of generation of NO and the rate constant expressed on a per mole of vanadium basis. The value of the rate constant calculated from the experimental data was then used to compute the rate of reaction at a standard condition, chosen as 2500 ppm NO, the typical inlet concentration of NO. At the low vanadium loadings, 1–6.4 wt% V, of these catalysts, 100% dispersion and accessibility was assumed, and every atom of vanadium was counted as an active site in calculating the TOFs. Thus, TOFs were calculated as:

$$\text{TOF} \equiv \left(-r^{\text{STD}}_{NO}\right) \quad C^{\text{STD}}_{NO} = \frac{v_0 C^{\text{STD}}_{NO}(-\ln(1-x))}{N_V} \tag{5}$$

where x is the conversion of NO through the reactor, v_0 is the volumetric flow rate of gases fed to the reactor, and N_V is the total number of mol of vanadium in the catalyst.

3. Results

3.1. Steady-state reaction

The vanadium loaded zeolite catalysts (VLZCs) used in steady-state reaction experiments are summarized in Table 1 along with a

Table 1
Table of vanadium-loaded zeolite catalysts

Catalyst	Host zeolite/ V precursor	Wt% V loading (from XRF)	Vanadium/ supercage [a]	Post reaction XRD results
VH_2Y–Cl	$H_2Y/VOCl_3$	1.26	0.40	Crystalline
		1.29	0.41	Crystalline
		1.60	0.53	Crystalline
		2.35	0.80	Crystalline
		4.06	1.44	Crystalline
		4.95	1.75	Crystalline
VH_6Y–Cl	$H_6Y/VOCl_3$	4.63	1.56	Amorphous after Rx
		4.97	1.66	Crystalline after Rx at 400°C. Moderately amorphous after reaction at 450°C
		6.16	2.10	Crystalline after Rx at 400°C. Slightly amorphous after reaction at 450°C

[a] Assuming vanadium present as VO and hydration during XRF measurement is 59 H_2O/unit cell.

qualitative measure of the post-reaction crystallinity of the zeolite framework determined from XRD patterns. The vanadium loading in these materials ranges from 1–6.4 wt% V, or 0.3–2.2 vanadium atoms per supercage on average. XRD patterns of the fresh, calcined catalysts often indicated moderate to significant levels of framework decomposition in the catalysts made from the H_6Y host zeolite, but the catalysts presented in Table 1 were all crystalline after calcination. All kinetic data presented in this paper correspond to catalysts whose zeolite framework remained intact throughout reaction. Data from catalysts whose structures collapsed during reaction were included in Table 1, but were otherwise omitted. Typically, the catalysts made from the H_2Y host were more stable at reaction conditions than those from H_6Y. Results in Table 1 indicate that several of the structures that collapsed at reaction temperatures of 450°C were found to be stable at 400°C. Fig. 1 compares the steady state TOFs of the catalysts made from the $VOCl_3$ precursor in each of the two acidic host zeolites, and shows the variations observed with loading in each case. Fig. 2 compares the selectivities of

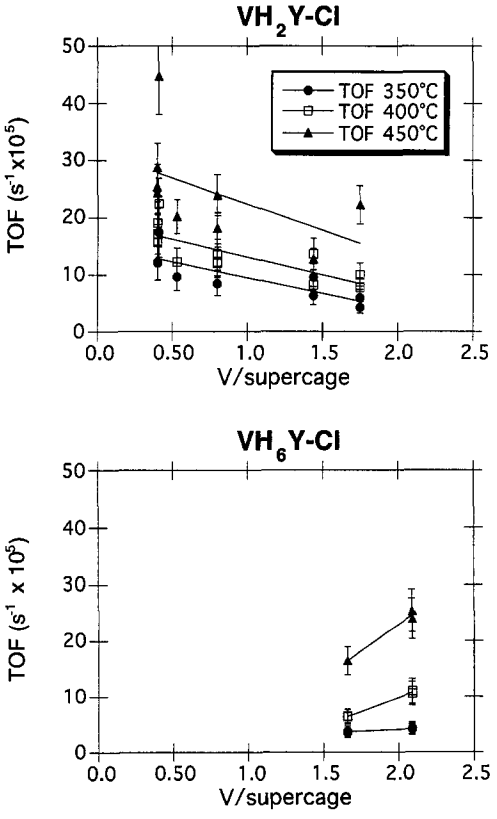

Fig. 1. TOF of NO reduction by NH_3 for VH_2Y–Cl and VH_6Y–Cl at 350, 400, and 450°C, and at various loadings of vanadium.

Table 2
Activation energies of vanadium-loaded zeolite catalysts

Catalyst	Mean E_a (kJ/mol)	E_a range (kJ/mol)
VH_2Y–Cl	35.9	27–53
VH_6Y–Cl	60.1	53–67
Supported Catalysts [26]		40–65

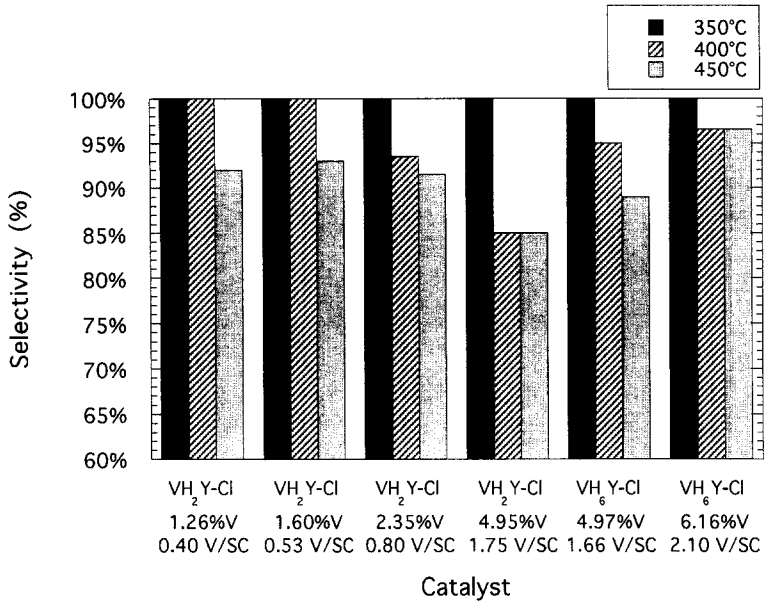

Fig. 2. Selectivity ($N_2/(N_2 + N_2O)$) for VH_2Y–Cl and VH_6Y–Cl at 350, 400, and 450°C for various loadings of vanadium.

VH_2Y–Cl and VH_6Y–Cl at the three reaction temperatures studied and at several loadings of vanadium. Effective activation energies of the VLZCs were calculated from Arrhenius plots, and are summarized in Table 2. There are several points worth making about the TOF and selectivity data presented in Fig. 1 and Fig. 2. The total variation in TOFs in the vanadium-loaded zeolite catalysts is relatively small, varying within an order of magnitude, from 1×10^{-5} to 3×10^{-4} mol NO/(mol V s). The TOFs of the VH_6Y–Cl catalysts increase with loading, which would support the hypothesis that interacting vanadium sites are more active. As the loading in the supercage increases, the likelihood of finding interacting vanadium centers increases which then increases the effective TOF of the catalyst. However, in the case of VH_2Y–Cl, the TOF decreases with loading. The high activity of this catalyst at low vanadium loading indicates that the isolated vanadium species in these materials are viable sites for NO reduction by NH_3. The selectivities of the VLZCs are at the high end of the range, 75–100%, reported for supported catalysts at similar temperatures. Fig. 2 also shows that the selectivity decreases with both temperature and loading, trends which are also observed in the selectivities of supported catalysts [1,8,9].

An important question is whether the vanadium-loaded zeolites can serve as model catalysts for the SCR system. To address this question, Fig. 3 shows a comparison of the TOFs for VH_2Y–Cl (1.26 wt% V, 0.4 V/SC), taken as a representative of the VLZCs, and several supported catalysts reported in the literature. This list is by no means complete, but does indicate the range of TOFs reported for supported catalysts used for mechanistic studies. The figure indicates that while the TOFs for the vanadium loaded zeolite catalysts are low when compared to the state-of-the-art supported catalyst, they are comparable to many of the supported catalysts in the literature. Furthermore, Janssen et al. [2,3] have shown that vanadium on silica–alumina (perhaps the best comparison to the zeolite support) behaves much like vanadium on alumina. We also note that NO reduction by NH_3 has been observed over vanadium incorporated in high-silica pentasil zeolites with a TOF of 2.2×10^{-3} s^{-1} at 300°C but with NO and NH_3 at 10000 ppm [28]. While the rates are

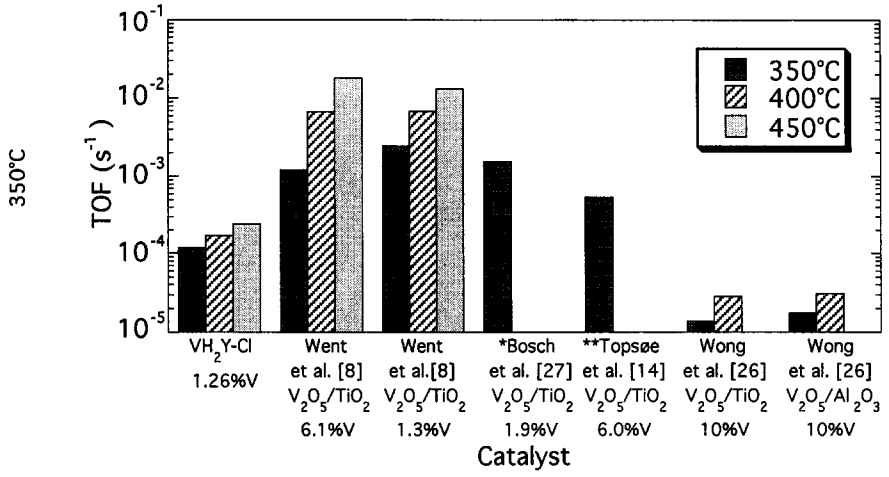

Fig. 3. Comparison of TOFs for NO reduction by NH_3 between vanadium-loaded zeolite catalyst and supported catalysts. (* Data from Bosch et al. [27] collected in 500 ppm O_2) (** Data from Topsøe et al. [14] collected at 250°C (TOF = 1.57×10^{-3}), TOF at 350°C estimated by assuming an activation energy of 50 kJ/mol)

comparable to those we have found for VLZCs, the work of Miyamoto et al. [28] showed higher TOF for less crystalline material and a decrease in TOF with the addition of oxygen. Preliminary experiments with our catalysts show an increase in TOF with addition of 500 to 3500 ppm of oxygen to the feed.

From the results presented in Table 2, it is clear that the activation energy of the VH_6Y–Cl catalysts are within the same range as the supported catalysts. The VH_2Y–Cl catalysts, however, show activation energies which are significantly lower than the rest of the VLZCs and the supported catalysts. Diffusion limitation in these materials was investigated as a possible explanation of the low activation energy of these materials. The Thiele modulus and effectiveness factor of the VLZCs were estimated for the first order reaction by assuming spherical particles of radii on the order of microns to hundreds of microns and an effective diffusivity for NO of 5.7×10^{-4} cm^2/s, based on Knudsen diffusivity through 7.4 Å pores. In all cases, the Thiele modulus, Φ_s, was $\ll 1$, and the effectiveness factor, η, $= 1$, indicating that these materials are not diffusion limited. This conclusion is supported by the observation that in the VH_2Y–Cl catalysts, as the loading is increased, the activation energy generally increases, as shown the Arrhenius plots in Fig. 4. If diffusion were indeed limiting the observed rate of reaction, this effect would increase as the cages became more crowded and the activation energy would decrease with loading. Thus, we ascribe the low activation energy to the chemical nature of the catalysts, but cannot yet invoke a mechanism for the barrier lowering.

3.2. Catalyst characterization

3.2.1. XPS

To ensure that the kinetic measurements correspond to intact zeolite samples, we have ex-

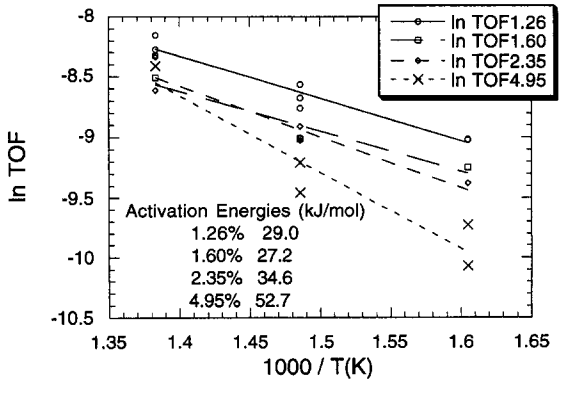

Fig. 4. Arrhenius plots used to calculate apparent activation energies for VH_2Y–Cl catalysts.

amined the most reactive samples by both XRD and XPS. XRD confirms crystallinity in the samples as we have already mentioned. The XPS measurements take advantage of the fact that the limited mean free path of the core electrons that are detected makes XPS a surface sensitive technique. In zeolites, the mean free path of these electrons is about 30–50 Å [29], which is equivalent to 3–4 supercages into the zeolite structure. Electrons ejected from within this layer account for more than 60% of the observed signal. The maximum XPS sampling depth in zeolites is on the order of 150 Å. XPS can then be used to monitor the possible migration of vanadium species out of the cages of the zeolite framework to the surface of the crystallites before and after reaction. Vanadium concentrations near the surface of the zeolite crystallites estimated from the XPS intensity ratios are reported in Table 3. Some of the catalysts showed some surface enrichment of vanadium before and/or following reaction, however, calculations showed that migration of only about 1–4% of the total vanadium into the XPS detection layer would account for the levels of surface enrichment observed. These calculations assumed homogeneous distribution of vanadium throughout a spherical crystallite, 1 μm in diameter. From this model, the amount of vanadium inside and outside the XPS detection layer were compared, and the migration of vanadium from the interior of the crystallite to the surface necessary to produce the given surface enrichment was calculated.

3.2.2. *Interpretation of NMR lineshapes*

Some background concerning the interpretation of the NMR lineshapes and the type of structural information available with ^{51}V-NMR is necessary to provide a context for the interpretation of the NMR results. The two main interactions which affect the NMR lineshape of solid state vanadium species are quadrupolar interactions and chemical shift anisotropy (CSA). Fortunately, these interactions have opposite dependencies on the applied magnetic field strength. When the strength of the applied magnetic field is increased, the CSA interactions begin to dominate the quadrupolar interactions, and at 9.4 T it has been shown that the quadrupolar interactions are negligible, and the lineshapes may be interpreted based on CSA of the central transition $(+1/2, -1/2)$ alone [23,24]. It was found that the anisotropy, δ_σ, (related to the width of the powder pattern), and the lineshape of the powder pattern were more reliable for distinguishing vanadium species in different coordination geometries than the isotropic chemical shift. Distorted tetrahedral and distorted octahedral coordination environments are distinguished based on the symmetry and anisotropy of the powder pattern. The tetrahedral environments can also be distinguished further according to the number of oxygen bridge bonds [23]. The NMR lineshape of the orthovanadate species with no oxygen bridge bonds is very symmetric with a very narrow anisotropy ($\delta_\sigma < 50$ ppm). There is a systematic increase in the anisotropy and asymmetry of the

Table 3
Surface concentration of vanadium measured by XPS

Catalyst	Bulk wt% V loading (XRF)	Vanadium atoms per supercage	Surface wt% V (XPS)	
			fresh, calcined	after reaction
VH_2Y–Cl	1.26	0.40		4.0
	1.29	0.41	4.2	
	2.35	0.80	6.0	
	4.06	1.44	4.3	
	4.95	1.75	5.0	6.0
VH_6Y–Cl	4.97	1.66		4.2

NMR lineshape as the number of oxygen bridge bonds per vanadium increases from the orthovanadate species to the pyrovanadate species ($\delta_\sigma \approx 90$–110 ppm), with one oxygen bridge bond, to the metavanadate species ($\delta_\sigma \approx 250$–$350$ ppm), with two oxygen bridge bonds. The NMR lineshapes of the distorted octahedral (6 coordinate) and square pyramid (5 coordinate) species are very different than those of the distorted tetrahedral species. These lineshapes have anisotropies ($\delta_\sigma \approx 450$–$650$ ppm) much larger than the widest tetrahedral lineshapes, and symmetries which correspond to environments that are nearly axially symmetric. Fig. 5 shows the ^{51}V-NMR wideline spectra of V_2O_5, NH_4VO_3, and Mg_3VO_4 model compounds obtained on our spectrometer. The ideal lineshapes of the central transitions of V_2O_5 and NH_4VO_3, calculated with a computer simulation program, are shown below the experimental spectra of these compounds in Fig. 5. The V_2O_5 simulated spectrum was computed from the following parameters: isotropic shift, δ_{iso}, $= -609$ ppm, anisotropy, δ_σ, $= 645$ ppm, asymmetry parameter, η_σ, $= 0.11$, and 2000 Hz line broadening imposed on the FID before Fourier transformation. These parameters describe the chemical shift anisotopy tensor in its principal axis system (PAS) [30]. The NH_4VO_3 simulated spectrum was computed from: $\delta_{iso} = -572$ ppm, $\delta_\sigma = 239$ ppm, $\eta_\sigma = 0.638$, and 5000 Hz line broadening. These parameters are similar to those reported by Eckert and Wachs [23], and Skibsted et al. [30]. The computer simulation program was written based on the theory outlined by Skibsted et al. [30]. The weak maximum in the experimental V_2O_5 spectrum in Fig. 5 is a contribution from the $(\pm 3/2, \pm 1/2)$ quadrupolar satellite transition. The differences between the experimental and computer simulated spectra of NH_4VO_3, including the sharp peaks at the singularities of the powder pattern and the shoulder near -1100 ppm, can also be explained by quadrupolar effects and instrumental nonidealities. Despite these differences, the experimental and simulated spectra in Fig. 5 illustrate the differences in the NMR lineshape corresponding to different vanadium environments, as established by Eckert and coworkers [23,24,31].

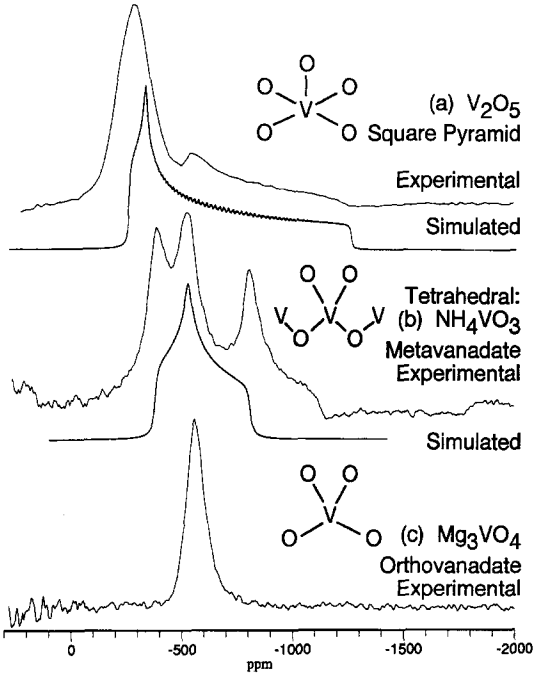

Fig. 5. ^{51}V-NMR results showing the variation in lineshape with vanadium coordination for vanadium model compounds: (a) V_2O_5 distorted octahedral: experimental spectrum and computer simulated central transition, (b) NH_4VO_3 tetrahedral metavanadate: experimental spectrum and computer simulated central transition, (c) Mg_3VO_4 tetrahedral orthovanadate: experimental spectrum.

3.2.3. NMR: VH_2Y–Cl

Fig. 6 shows the variation in ^{51}V-NMR lineshape with vanadium loading for the calcined VH_2Y–Cl catalysts. All the spectra in this figure where collected under Magic Angle Spinning (MAS) conditions. This technique orients the axis of the NMR rotor at an angle of 54°44′ (the magic angle, θ: $(3\cos^2\theta - 1) = 0$) with respect to the external magnetic field. The Fourier transformation of the modulation caused by the rotation of the sample breaks the wideline powder pattern into a set of spinning side bands (SSBs). The tips of the SSBs roughly trace out the original powder pattern. This means

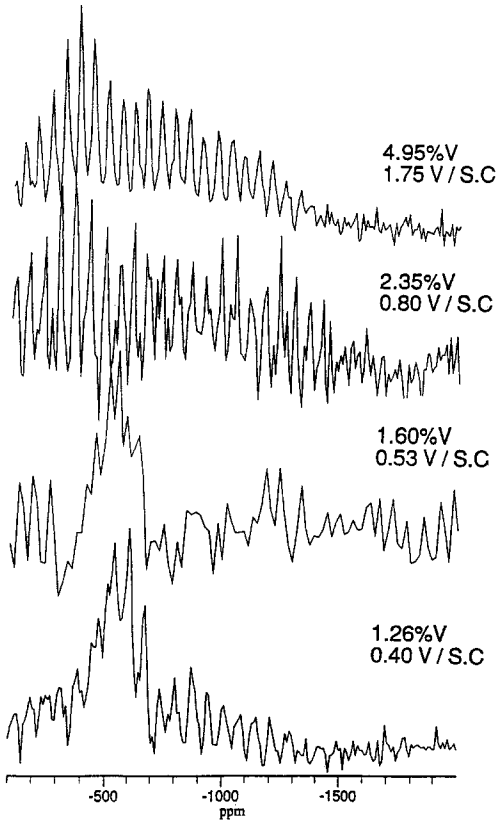

Fig. 6. ^{51}V-NMR results showing the variation in lineshape with vanadium loading for the VH_2Y–Cl catalysts. (a–d from bottom up)

that interpretation of the envelope of the SSBs in terms of chemical shift anisotropy can be done just as with wideline spectra above. MAS also increases signal-to-noise (since spectral area is conserved), which is especially important in these spectra since the signal-to-noise is relatively poor because the concentrations of vanadium are low.

Fig. 6a and 6b correspond to the lower loadings of vanadium in the VH_2Y–Cl catalysts and show lineshapes typical of isolated tetrahedrally coordinated vanadium species, with a chemical shift of about −540 ppm. As the loading is increased, Fig. 6c and 6d, there is a transition from the isolated tetrahedral to a distorted octahedral or square pyramid coordination of the vanadium. The NMR lineshape and SSB pattern of Fig. 6d is very similar to that of crystalline V_2O_5. This trend of tetrahedrally coordinated vanadium at low loadings and distorted octahedral or square pyramid coordinations at high loadings has also been observed in this work for other VLZCs.

3.2.4. NMR: VH_6Y–Cl

Fig. 7 shows the NMR results for the VH_6Y–Cl catalyst at a loading of 2.1 V/SC. The bottom spectrum, Fig. 7a, corresponds to the calcined sample in which every effort was taken to limit its exposure to the atmosphere. Fig. 7b–d correspond to sequential thermal treatments. Before each treatment, the catalyst was removed from the NMR rotor, given the thermal treatment indicated, returned to the NMR rotor, and again isolated from the atmosphere with O-ring end caps. During transfers between the rotor and furnace, the catalyst was exposed to the atmosphere for periods of less than 5 min each way. The spectra in Fig. 7, although collected under MAS conditions, do not show SSBs, except for the spectrum in Fig. 7a, in

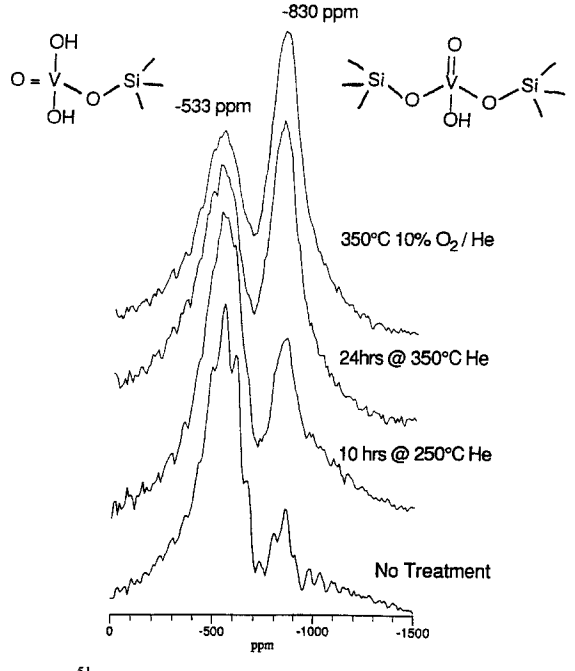

Fig. 7. ^{51}V-NMR results showing the variation in lineshape following sequential thermal treatments for the 6.4%V VH_6Y–Cl catalysts (a–d from bottom up).

which only the tips of the SSBs are resolved. The resonance lineshapes are relatively symmetric about each maximum, at −533 and −830 ppm, and have been assigned to two distinct vanadium environments, differing in chemical shift, but not differing much in chemical shift anisotropy. The symmetries of these lines indicate that each of the vanadium species is isolated and tetrahedrally coordinated since their NMR powder patterns do not have the asymmetry usually associated with pyrovanadate dimers or polyvanadate chains. The wider linewidths compared to orthovanadate model compounds indicate that the vanadium environment is slightly heterogeneous. Such heterogeneity can be accounted for by disorder, perhaps a distribution of bond lengths or bond angles, throughout the sample. This would lead to a distribution of isotropic shifts, for example, and translate into an increased linewidth when compared to the ordered environment found in the orthovanadate model compounds. A distribution of isotropic shifts would also prevent the resolution of the SSBs if the range of the distribution is on the order of the MAS spinning speed. The spectra also indicate that the thermal treatments facilitate a transition from the species at −530 ppm to the species at −830 ppm. These species have tentatively been assigned as differing in the number of bonds that the vanadium species has with the zeolite framework, such that the −830 ppm species is more strongly bound to the zeolite framework, possibly with two or more bonds, while the −530 ppm species is bound with only one bond to the framework. These interpretations are consistent with work done by Lapina and coworkers [32,33] with ^{51}V-NMR of V_2O_5/Al_2O_3 catalysts. Lapina and coworkers observed two distinct tetrahedral vanadia species on the alumina surface, one with an isotropic chemical shift in the range of −500 to −550 ppm and the other with an isotropic chemical shift near −750. They also observed that stronger thermal treatments increased the intensity of the −750 species, which was assigned to an isolated tetrahedral species which was more strongly bound to the alumina surface, completely analogous to the interpretations of our results.

3.2.5. EXAFS: VH_6Y–Cl

The combination of XANES (X-ray absorption near edge structure) and EXAFS (extended X-ray absorption fine structure) data can also yield information about the local site geometry in a sample. Fig. 8 shows the XANES (inset) and Fourier transformed EXAFS data (k weighted) for VH_6Y–Cl (6.4 wt%) after calcination at 350°C (the sample corresponding to the NMR spectrum in Fig. 7a). Strong and narrow pre-edges as seen in the XANES spectrum are usually indicative of vanadium being coordinated either fivefold in a tetragonal square pyramid as in V_2O_5, or of a tetrahedral coordination as in NH_4VO_3. The corresponding 1s → 3d transition is strictly dipole forbidden in a regular octahedral environment and small pre-edges only become visible upon lowering the site symmetry. However, in tetrahedrally coordinated vanadium this transition becomes dipole allowed. Wong et al. [34] found the most intense pre-edges in tetrahedral compounds like metavanadate, while V_2O_5 exhibits a slightly smaller peak height. In the VH_6Y–Cl sample the pre-edge is slightly smaller than for V_2O_5

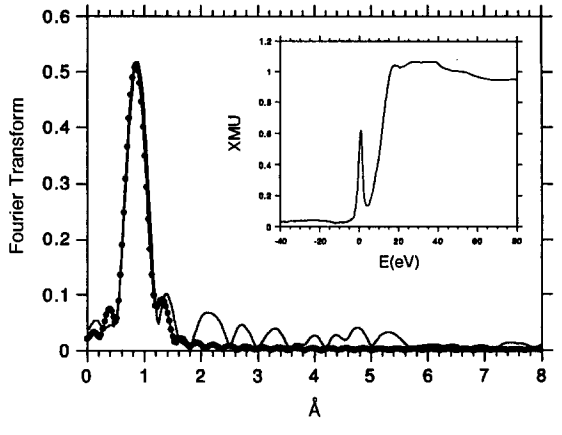

Fig. 8. Fourier transformed EXAFS data (k-weighted, 2.9–13.3 Å^{-1}) of 6.4 wt% V VH_6Y–Cl, calcined at 350°C (solid line) and fit (line with dots). Inset: XANES region of this sample.

such that a distinction between tetrahedral and square pyramidal coordination cannot be made on this basis alone. However, the EXAFS spectrum reveals only one major peak that could be fitted with the $VOCl_3$ reference (V=O at 1.57 Å [35]) to result in four V–O bonds at a distance of 1.56 Å. An overlay of the fitted results is shown in Fig. 8 (fit = line with dots). It can be seen that no major additional contribution exists that could be distinguished from noise. The predominance of one bond distance is also reflected in the width of the pre-edge: Wong et al. found a correlation of the width of the pre-edge at half height with the spread in bond distances. Our sample exhibits a width of 2.71 eV, which is considerably smaller than the 3.4 eV we find in V_2O_5 and close to the 2.55 eV width that we find for metavanadate.

Based on the above, and the NMR results, we suggest that vanadium in this sample resides predominantly in the form of a tetrahedral vanadate ion, that is probably linked to the zeolite framework through a single oxide bridge. This would also explain that no ordered framework attachment is visible in the EXAFS spectrum.

3.3. Diffuse reflectance FTIR (DRIFTS)

Fig. 9 and Fig. 10 show the DRIFTS results for the VH_2Y–Cl catalyst with a vanadium loading of 0.41 V/SC. Fig. 9 shows the stretching region while Fig. 10 shows the bending and deformation region. These spectra correspond to ammonia adsorption on the catalyst at 100°C (a), followed by a nitrogen purge in an attempt to remove gas phase and physically adsorbed species (b). Then the catalyst with preadsorbed ammonia was exposed to a flow of NO and NH_3 (40 cc/min, 2500 ppm NO, 2500 ppm NH_3, balance He) at 100°C (c). The spectra show IR absorption bands which have been assigned to molecular water, gas phase ammonia, and ammonia chemisorbed on Lewis acid sites and on Brønsted acid sites as ammonium ions. Bands belonging to the ammonium ions are assigned as: 1400–1450 cm^{-1} (antisymmetric deformations), 1700 cm^{-1} (symmetric deformations), and 3045 and 2820 cm^{-1} (symmetric and antisymmetric N–H stretching). Bands at 1640 and 3500–3300 cm^{-1} are assigned to the H–O–H deformation and O–H stretching modes, respectively, of molecular water adsorbed within the zeolite framework. Gas phase ammonia is identified by the bands at 1625 cm^{-1} (antisymmetric deformation), 3334 cm^{-1} (symmetric N–H stretching), and 966, 931 cm^{-1} (symmetric deformation split by inversion doubling) [36]. Absorption bands in the range 3300–3100 cm^{-1}, shown in Fig. 9, may be assigned either to physically adsorbed ammonia that was not removed by the nitrogen purge or

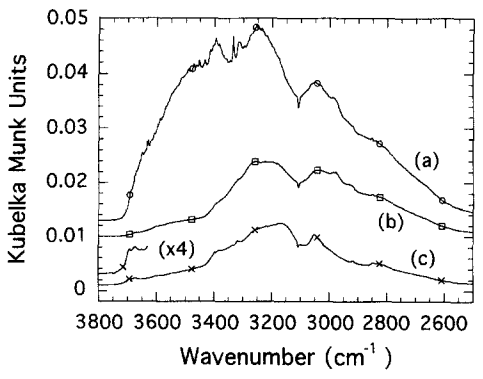

Fig. 9. DRIFTS results in the stretching region of the infrared spectrum, for the 1.29% V VH_2Y–Cl catalyst at 100°C during adsorption of NH_3 (a), following N_2 purge of reaction cell (b), and during in situ reaction of NO with the preadsorbed NH_3 (c). Expansion shows –OH stretching region of spectrum (c).

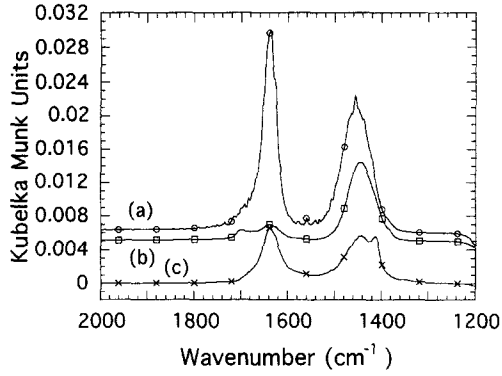

Fig. 10. DRIFTS results in the bending region of the infrared spectrum, for the 1.29% V VH_2Y–Cl catalyst at 100°C during adsorption of NH_3 (a), following N_2 purge of reaction cell (b), and during in situ reaction of NO with the preadsorbed NH_3 (c).

ammonia coordinated to Lewis acid sites. Other bands typically found with Lewis bound ammonia, the antisymmetric deformation band at 1600 cm^{-1}, and the symmetric deformation band at 1150–1280 cm^{-1} were not detected in either the single beam or ratioed spectra at these temperatures. The majority of the intensity in the range 3400–3100 cm^{-1} was removed by the nitrogen purge, and therefore, is assigned to physically adsorbed ammonia. However, the weak bands at 3393, 3314, and 3250 cm^{-1}, which remained even at high temperatures, correspond to ammonia bound to Lewis acid sites. The spectra in Fig. 10 contain two bands in the region between 1400–1450 cm^{-1}, at 1450 and 1408 cm^{-1}. These bands, resolved more clearly in Fig. 10c, are assigned to ammonium ions on Brønsted acid sites of different acid strengths. When ammonia is adsorbed on the unloaded acid zeolites, a band is observed at 1450 cm^{-1} corresponding to chemisorption of ammonia on zeolite Brønsted acid sites. The 1450 cm^{-1} band in VH_2Y–Cl is therefore assigned to a zeolite Brønsted acid site while the 1408 cm^{-1} band may be an ammonium ion adsorbed on a Brønsted acid site associated with a vanadium species. Infrared bands of ammonium ions adsorbed on Brønsted acid sites associated with vanadia species on supported catalytic materials were reported at 1410 cm^{-1} by Inomata et al. [16] and Takagi et al. [37], and at 1430 cm^{-1} by Topsøe et al. [12–14] and Schneider et al. [38], supporting the assignments made here.

When the catalyst with preadsorbed ammonia is exposed to a flow of NO/NH_3 at 100°C after the N_2 purge, several changes are apparent. The bands assigned to molecular water increase, and the bands assigned to ammonium ions decrease, indicating that the NO is reacting with the preadsorbed ammonia through the SCR reaction pathway. There is also a new hydroxyl band at 3690 cm^{-1}, shown in the expansion of Fig. 9c. This band has also been observed by Topsøe [13,14] during similar experiments over V_2O_5/TiO_2 catalysts, and was assigned as a hydroxyl on a reduced vanadium center, V^{+4}–OH. Thus, NO is reacting with the activated ammonia species, generating nitrogen and water as reaction products, and leaving the vanadium in a reduced state. In the absence of gas phase oxygen, the reoxidation step by NO is rate limiting, and may not proceed at an observable rate at 100°C. We note that we did not see the 2040 cm^{-1} V=O overtone band seen by Topsøe et al. [14] on V_2O_5/TiO_2 catalysts.

4. Conclusions

Characterization of the zeolite encapsulated vanadium oxo species with NMR and EXAFS shows that the zeolite hosts generally encapsulate the vanadium as isolated, distorted tetrahedral oxo species. There is no clear NMR or EXAFS evidence for V–O–V bonds in the tetrahedral species in these materials. NMR data show evidence for two distinct isolated tetrahedral species, having different chemical shifts but similar chemical shift anisotropies. Thermal treatment, possibly in the presence of small amounts of water adsorbed from the atmosphere, has been shown to facilitate the transition from the species at −530 ppm to the species at −830 ppm. These species have been tentatively assigned as differing in the number of bonds that the vanadium center has with the zeolite framework. In this model, the −830 ppm species is more tightly bound to the framework, perhaps with two Si–O–V bonds, while the −530 ppm species has only one such bond. The EXAFS results support the NMR assignment of the vanadium species as 4 coordinate. The NMR results indicate that the zeolite hosts can also encapsulate the vanadium species as either distorted octahedral or square pyramidal species, especially at higher loadings of vanadium. The NMR lineshape and SSB pattern of the square pyramidal species indicates that the local environment of this species resembles that of V_2O_5.

The DRIFTS ammonia adsorption experiments indicate that the VLZCs adsorb ammonia

mainly on Brønsted acid sites as ammonium ions. There is evidence for two Brønsted acid sites in these materials. These sites have been assigned as corresponding to a zeolite Brønsted acid site generating the band at 1450 cm^{-1} and a Brønsted acid site associated with the vanadium species generating a band at 1408 cm^{-1}. These assignments are supported by comparisons of the IR frequencies with those observed when ammonia is adsorbed on unloaded acid zeolites giving a single ammonium species with a IR band at 1450 cm^{-1}. Lewis acid sites are also observed in these materials, especially at higher temperatures. In situ DRIFTS results showed that low temperature reaction between NO and NH_3 generated a hydroxyl species and molecular water as a reaction product, and consumed ammonium ions. The hydroxyl species showed a band at 3690 cm^{-1} and was assigned to a hydroxyl on a reduced vanadium center in accordance with the literature. All of the changes caused by the interaction of NO with the adsorbed ammonia are consistent with progress through the reaction pathway.

The vanadium loaded zeolite catalysts in this work show catalytic properties for NO reduction by NH_3 that are very similar to those of other supported catalysts found in the literature. The activation energies of the VH_6Y–Cl catalysts fall within the range of activation energies of the supported catalysts. The selectivities of the model catalysts are at the high end of the supported catalyst range, and they follow the same trends with temperature and loading as the supported catalysts. TOFs of the VLZCs are low with respect to the state-of-the-art supported catalysts, but are comparable to many of the supported catalysts used for mechanistic studies found in the literature. The VH_2Y–Cl catalysts seem to be unique. They are the most active, most selective, and most stable catalysts, and have the lowest activation energy and the interesting trend that the TOFs decrease with vanadium loading. XPS results show that the surface vanadium concentration is essentially the same as the bulk concentration before reaction, indicating that the vanadium is indeed within the zeolite framework. XPS results following reaction indicate some V mobility, but the resulting changes in surface concentration represent a minor, often negligible, fraction of the total vanadium. X-ray diffraction patterns show that the zeolite framework structure often remains stable at reaction conditions. Catalysts with high loadings of vanadium and catalysts made from the H_6Y host zeolites tend to be less stable. All of the similarities in the catalytic properties of the VLZCs and supported catalysts imply that the former materials may be useful model catalysts for the SCR reaction and that isolated vanadyl species, perhaps near a zeolite acid site, are viable sites for reduction of NO with ammonia.

Acknowledgements

Funding from the US Department of Energy for part of this work is gratefully acknowledged. The operational funds for the NSLS beamline X-11A are supported by DOE grant DE-AS0580ER10742.

References

[1] H. Bosch and F. Janssen, Catal. Today 2 (1988) 369.
[2] F. Janssen, F. van den Kerkhof, H. Bosch and J. Ross, J. Phys. Chem. 91 (1987) 5921.
[3] F. Janssen, F. van den Kerkhof, H. Bosch and J. Ross, J. Phys. Chem. 91 (1987) 6633.
[4] G. Ramis, G. Busca, F. Bregani and P. Forzatti, Appl. Catal. 64 (1990) 243.
[5] G. Ramis, G. Busca, F. Bregani and P. Forzatti, Appl. Catal. 64 (1990) 259.
[6] G. Busca, H. Saussey, O. Saur, J. Lavalley and V. Lorenzelli, Appl. Catal. 14 (1985) 245.
[7] L. Lietti, J. Svachula, P. Forzatti, G. Busca, G. Ramis and F. Bregani, Catal. Today 17 (1993) 131.
[8] G. Went, L. Leu, R. Rosin and A. Bell, J. Catal. 134 (1992) 492.
[9] G.Went, L. Leu and A. Bell, J. Catal. 134 (1992) 497.
[10] J. Odriozola, H. Heinemann, G. Somorjai, J. Garcia de la Banda and P. Pereira, J. Catal. 119 (1989) 71.
[11] J. Odriozola, J. Soria, G. Somorjai, H. Heinemann, J. Garcia de la Banda, M. Lopez Granados and J. Conesa, J. Phys. Chem. 95 (1991) 240.

[12] N.-Y. Topsøe, J. Catal. 128 (1991) 499.
[13] N.-Y. Topsøe, H. Topsøe and J. Dumesic, J. Catal. 151 (1995) 226.
[14] N.-Y. Topsøe, J. Dumesic and H. Topsøe, J. Catal. 151 (1995) 241.
[15] A. Miyamoto, K. Kobayashi, M. Inomata and Y. Murakami, J. Phys. Chem. 86 (1982) 2945.
[16] M. Inomata, A. Miyamoto and Y. Murakami, J. Catal. 62 (1980) 140.
[17] M. Gaisor, J. Haber, T. Machej and T. Czeppe, J. Mol. Catal. 43 (1988) 359.
[18] M. Takagi, T. Kawai, M. Soma, T. Onishi and K. Tamaru, J. Catal. 50 (1977) 441.
[19] M. Takagi, T. Kawai, M. Soma, T. Onishi and K. Tamaru, J. Catal. 57 (1979) 528.
[20] R. Rajadhyaksha and M. Knözinger, Appl. Catal. 51 (1989) 81.
[21] U. Ozkan, Y. Cai and M. Kumthekar, Appl. Catal. A: General 96 (1993) 365.
[22] J. Scofield, J. Electron Spectrosc. 8 (1976) 129.
[23] H. Eckert and I.E. Wachs, J. Phys. Chem. 93 (18) (1989) 6796.
[24] H. Eckert, G. Deo, I.E. Wachs and A.M. Hirt, Colloids Surf. 45 (1990) 347.
[25] K. Moller, A. Borvonwattananout and T. Bein, J. Phys. Chem 93 (1989) 4562.
[26] W. Wong and K. Nobe, Ind. Eng. Chem. Prod. Res. Dev. 25 (1986) 179.
[27] H. Bosch, F. Janssen, F. van den Kerkhof, J. Oldenziel, J. Ommen and J. Ross, Appl. Catal. 25 (1986) 239.
[28] A. Miyamoto, D. Medhanavyn and T. Inui, In: eds. M.J. Phillips and M. Ternan, Proc. of the Ninth Int. Congr. on Catal. (The Chemical Institute of Canada, Ottawa, 1988) p. 435.
[29] L. Pedersen and J. Lunsford, J. Catal. 61 (1980) 39.
[30] J. Skibsted, N.C. Nielsen, H. Bildsoe and H.J. Jakobsen, Chem. Phys. Lett. 188 (5) (1992) 405.
[31] H. Eckert, In: eds. A. Bell and A. Pines, NMR Techniques in Catalysis (Marcel Dekker, New York) Ch. 4, p. 195.
[32] O. Lapina, V. Mastikhin, L. Simonova and Y. Bulgakova, J. Mol. Catal. 69 (1991) 61.
[33] Z. Sobalik, M. Markvart, P. Stopka, O. Lapina and V. Mastikhin, J. Mol. Catal. 71 (1992) 69.
[34] J. Wong, F. Lytle, R. Messmer and D. Maylotte, Phys. Rev. B 30 (10) (1984) 5596.
[35] K. Palmer, J. Am. Chem. Soc. 60 (1938) 2360.
[36] K. Nakamoto, Infrared Spectra of Inorganic and Coordination Compounds (Wiley, New York, 1978) p. 85.
[37] M. Takagi, M. Soma, T. Onishi and K. Tamaru, Can. J. Chem. 58 (1980) 2132.
[38] H. Schneider, S. Tschudin, M. Schneider, A. Wokaun and A. Baiker, J Catal. 147 (1994) 5.